Nano Research 2018, 11(8): 4215–4224
https://doi.org/10.1007/s12274-018-2009-9
Research Article
ISSN 1998-0124
CN 11-5974/O4

Ultrasensitive H_2S gas sensors based on p-type WS_2 hybrid materials

Georgies Alene Asres[1], José J. Baldoví[2,3], Aron Dombovari[1], Topias Järvinen[1], Gabriela Simone Lorite[1], Melinda Mohl[1], Andrey Shchukarev[4], Alejandro Pérez Paz[3,5], Lede Xian[2,3], Jyri-Pekka Mikkola[4,6], Anita Lloyd Spetz[1,7], Heli Jantunen[1], Ángel Rubio[2,3] (✉), and Krisztian Kordas[1] (✉)

[1] *Microelectronics Research Unit, Faculty of Information Technology and Electrical Engineering, University of Oulu, P.O. Box 4500, FI-90014 Oulu, Finland*
[2] *Max Planck Institute for the Structure and Dynamics of Matter, Luruper Chaussee 149, 22761 Hamburg, Germany*
[3] *Nano-Bio Spectroscopy Group, European Theoretical Spectroscopy Facility (ETSF), Universidad del País Vasco, CFM SCIC-UPV/EHU-MPC DIPC, Avenida Tolosa 72, 20018 San Sebastian, Spain*
[4] *Technical Chemistry, Department of Chemistry, Chemical-Biological Centre, Umeå University, SE-90187 Umeå, Sweden*
[5] *School of Chemical Sciences and Engineering, School of Physics and Nanotechnology, Yachay Tech University, Urcuquí, Ecuador*
[6] *Industrial Chemistry & Reaction Engineering, Department of Chemical Engineering, Johan Gadolin Process Chemistry Centre, Åbo Akademi University, FI-20500 Åbo-Turku, Finland*
[7] *Sensor and Actuator Systems, Department of Physics, Chemistry and Biology, Linköping University, SE-58183 Linköping, Sweden*

Received: 16 November 2017
Revised: 23 January 2018
Accepted: 27 January 2018

KEYWORDS

WS_2,
nanowire,
nanoflake,
gas sensor,
H_2S,
O doping

ABSTRACT

Owing to their higher intrinsic electrical conductivity and chemical stability with respect to their oxide counterparts, nanostructured metal sulfides are expected to revive materials for resistive chemical sensor applications. Herein, we explore the gas sensing behavior of WS_2 nanowire-nanoflake hybrid materials and demonstrate their excellent sensitivity (0.043 ppm^{-1}) as well as high selectivity towards H_2S relative to CO, NH_3, H_2, and NO (with corresponding sensitivities of 0.002, 0.0074, 0.0002, and 0.0046 ppm^{-1}, respectively). Gas response measurements, complemented with the results of X-ray photoelectron spectroscopy analysis and first-principles calculations based on density functional theory, suggest that the intrinsic electronic properties of pristine WS_2 alone are not sufficient to explain the observed high sensitivity towards H_2S. A major role in this behavior is also played by O doping in the S sites of the WS_2 lattice. The results of the present study open up new avenues for the use of transition metal disulfide nanomaterials as effective alternatives to metal oxides in future applications for industrial process control, security, and health and environmental safety.

Address correspondence to Krisztian Kordas, krisztian.kordas@oulu.fi; Ángel Rubio, angel.rubio@mpsd.mpg.de

1 Introduction

Gases with different properties, origins, and concentrations are pervasive in our environment. Some of these gases are highly toxic and hazardous, while others are essential for life or indicators of health status. Accordingly, sensors for gas detection and monitoring are needed in various sectors such as environmental protection, industrial process monitoring and safety, amenity, energy saving, health, and food industries [1]. Metal oxide semiconductors stand out as the most common active sensing materials used in practical devices. Grain size reduction to the nanometer range and relatively easy sensitization to various analytes (via either lattice doping with anions and cations or surface decoration with metals and metal oxides) have emerged as key strategies to improve their detection properties [2, 3]. The main drawbacks of current metal oxide-based devices are associated with their typically high operating temperatures (several hundreds of degrees) and limited use in environments containing even traces of sulfur and sulfides, because of the easy poisoning of the catalytically active surfaces involved in the adsorption and sensing of analytes [4]. In principle, other types of gas sensors whose operation is based on, e.g., gas ionization [5] or changes in the optical properties of waveguides [6], may represent alternative solutions; however, their typical detection limits are at most a few parts per million of analyte. For this reason, and to further improve the existing sensing performance of resistive-type gas sensors, significant efforts are being directed towards developing new classes of materials that are less susceptible to poisoning, such as carbon nanotubes [7], graphene [8], conducting polymers [9], and transition metal dichalcogenide (TMD) nanostructures [10], to replace metal oxides.

Among the new types of nanoscopic sensors being studied, layered transition metal dichalcogenide (MX_2, M = Mo, W; X = S, Se) nanostructures have recently attracted significant interest. Often compared to graphene and other two-dimensional (2D) nanomaterials, their properties present distinct advantages for electronic, optical, and electrochemical sensors [11]. Recent studies, mostly focused on MoS_2 [12–15] and WS_2 [16, 17], highlighted the gas sensing applications associated with the large specific surface area of the TMD materials, particularly of those with a mono- or few-layered microstructure. Previous studies suggest that the working mechanism of TMD gas sensors involves charge transfer-based conductance modulation [11, 13, 18]. Since the electron density is dependent on the dimensions of the crystal lattice, it is reasonable to expect that the gas sensing properties are also influenced by the dimensions and microstructure of the sensing material. This motivated our very recent investigation of the gas sensing properties of nanowire-nanoflake hybrid WS_2 nanostructures [19].

Therefore, in this work, the gas sensing characteristics of WS_2 nanowire-nanoflake hybrid materials were investigated using a simple two-terminal Taguchi-type sensor arrangement, operating at moderate temperatures (30 and 200 ˚C). The sensors were exposed to five different analytes (H_2S, CO, NH_3, H_2, and NO buffered in air) and their response, sensitivity, and recovery properties were assessed. The goal was to obtain experimental evidence supporting previous gas sensitivity data predicted from modeling studies, and to compare the experimental measurements to more recent molecular dynamics simulation results. We show that the WS_2 nanowire-nanoflake hybrids have particularly high sensitivity towards H_2S, allowing detection and quantification of analyte concentrations on the order of parts per billion, competing with other known materials such as Fe_2O_3 nanochains and nanoparticles [20, 21], CuO-SnO_2 [22], CuO nanoparticles [23] and nanosheets [24], mesoporous WO_3 [25], CeO_2 nanowires [26], and PbS quantum dots [27] (for a comprehensive list, see Table S1 in the Electronic Supplementary Material (ESM)).

2 Experimental and modeling details

The WS_2 nanohybrids were synthesized according to the procedures detailed in our previous report [19]. In brief, WO_3 nanowires were first synthesized by hydrothermal recrystallization of $Na_2WO_4{\cdot}2H_2O$ in acidic environment at 180 ˚C under autogenic pressure, and then sulfurized at 800 ˚C for 10 min in sulfur vapor to convert them to WS_2 nanowire-nanoflake hybrids. The microstructure of the as-obtained materials was determined by field emission scanning electron

microscopy (FE-SEM, Zeiss Ultra Plus) and transmission electron microscopy (TEM, JEOL JEM-2200FS). The chemical surface composition of the nanomaterials was assessed by a Kratos Axis Ultra X-ray photoelectron spectrometer (with a monochromatic Al Kα source operated at 150 W) equipped with a delay line detector and a charge neutralizer. The spectra were processed with the Kratos software.

Two-terminal Taguchi-type resistive gas sensors were fabricated on test chips with Pt/Ti (300 nm/45 nm) microelectrodes on a Si/SiO_2 substrate (a 300 nm-thick thermal oxide deposited on B-doped p^+-Si). The electrode patterns were defined by optical lithography using the lift-off method. To prepare the sensor devices, a small amount (~ 20 mg) of the WS_2 nanowire/nanoflake hybrid powder was dispersed in 10 mL acetone by ultrasonication, then deposited between the platinum electrodes by drop casting, and finally dried under ambient conditions for 1 day before the gas sensing measurements. The amount of drop-cast material was chosen in such a way to produce a reasonable conductive active layer, with typical resistance values between 3 and 100 MΩ at room temperature.

The gas sensing measurements were performed by testing the chips in a Linkam TMS 94 gas flow chamber. The sample resistance was measured at a 1 V bias, using a computer-controlled Hewlett–Packard 3458 A multimeter. The sensor devices were tested at 30 and 200 °C on air-buffered analytes (H_2S, CO, NH_3, H_2, and NO) with nominal concentrations between 1 and 600 ppm, using a MKS Type 247 mass-flow controller. Some of the sensors were also tested on sub-ppm concentrations (between 10 and 1,000 ppb) of H_2S at 200 °C.

In addition, we performed first-principles calculations based on density functional theory (DFT), using the generalized gradient approximation (GGA) exchange-correlation functional of Perdew, Burke, and Ernzerhof (PBE) [28], as implemented in the Quantum Espresso code [29]. The important role of van der Waals (vdW) interactions in the layered structure of WS_2 was accounted for by including the Grimme's semiempirical dispersion correction (D2), which describes the vdW interactions by a pairwise force field [30]. We used norm-conserving Goedecker–Hartwigsen–Hutter–Teter pseudopotentials [31], whereas the electronic wavefunctions were expanded in a plane-wave basis set, with energy cutoffs of 90 and 360 Ry for the wavefunctions and the charge density, respectively. A 10×10×1 Monkhorst–Pack [32] grid was used for k-point sampling within a single unit cell of bulk WS_2. The total energy and the forces on each atom were converged to within 1 mRy/atom and 0.2 meV, respectively, thus allowing us to obtain a quantitative description of the sensing behavior of the 2D-based materials. Furthermore, 4×4 slabs were built to simulate the adsorption of an individual molecule of H_2S on both single-layer (32 S and 16 W atoms) and bilayer (64 S and 32 W atoms) WS_2, to take into account the possible intercalation of gas molecules between the adjacent layers. Due to the periodic boundary conditions, this geometry corresponds to 6.28×10^{13} molecules/cm^2 in the monolayer. The distance between two neighboring gas molecules was thus larger than 12 Å. In order to avoid unphysical interactions between images along the non-periodic direction, the distance between monolayers was set to ~ 20 Å, with a dipole correction layer. Integrations over the Brillouin zone were carried out using a regular mesh of 3×3×1 k-points for the structural relaxation of the slab, and at the zone center for a single molecule. A denser mesh of 6×6×1 k-points was used for the density of states (DOS) and Bader charge transfer calculations [33]. The calculations were also extended to study the adsorption of H_2, CO, NO, and NH_3 gases on the WS_2 monolayer; spin-polarized calculations were performed in the case of NO adsorption.

3 Results and discussion

The hydrothermally synthesized WO_3 samples were composed of precisely oriented nanowires, as revealed by the scanning and transmission electron microscopy measurements (Fig. 1(b)). Based on the high-resolution transmission electron microscopy (HRTEM) image in Fig. 1(c) and the selected area electron diffraction (SAED) pattern, the spacing of the lattice fringes was found to be 0.39 nm, which can be indexed as the (001) plane of hexagonal WO_3. This indicates that the growth of the nanowires occurred along the [001]

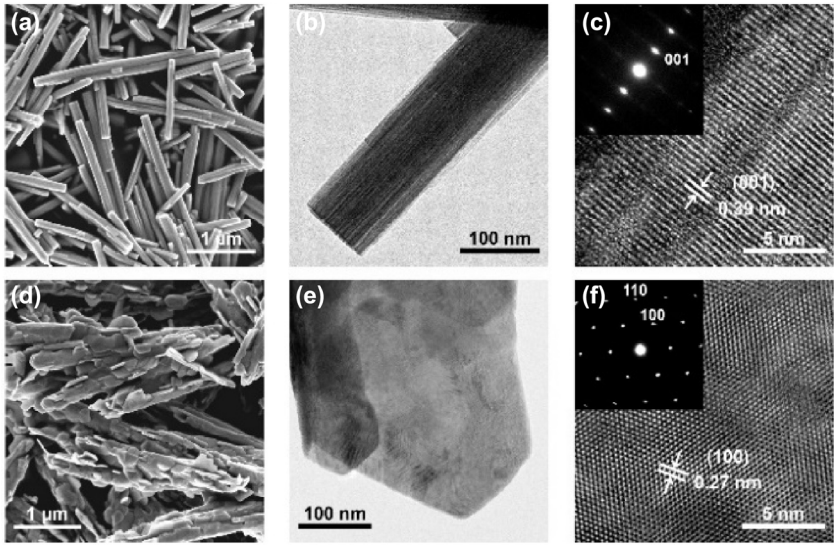

Figure 1 Microstructure of WO_3 nanowires and WS_2 nanowire/nanoflake hybrids. (a) and (d) Low-magnification SEM image, and (b) and (e) TEM images of WO_3 nanowires and WS_2 nanowire/nanoflake structures. (c) and (f) HRTEM images (with SAED pattern in the inset) of (c) a single WO_3 nanowire (zone axis [120]) and (f) a single WS_2 nanoflake (zone axis [001]).

direction. After sulfurization, the morphology and other characteristics of the as-formed WS_2 nanowire/nanoflake structure (Fig. 1(d)) were identical to those reported in our previous work. The hybrids consisted of elongated rod-shaped structures with partially peeled surfaces, thus forming nanoflakes (Fig. 1(e)) that are an integral part of the original nanorod [19]. The length of the hybrid structures is around 1–3 μm. Their core has a typical diameter of 200–300 nm, whereas the size of the partially peeled flakes is ~ 200 nm in diameter and 10 nm in thickness (Fig. 1). The high-resolution image of a single-crystal 2D WS_2 nanoflake (Fig. 1(f)) reveals crystal planes with a spacing of 0.27 nm, which can be indexed as the (100) plane of hexagonal WS_2.

Resistive gas sensor measurements of the WS_2 hybrid materials dispersed on the test chips indicated p-type semiconducting behavior, as the resistance increased for reducing gases (H_2S, CO, NH_3, and H_2) and decreased for nitric oxide, which is an oxidant (Fig. 2). In simple terms, the sensing mechanism is based on the localization of positive charge in the lattice by the surface-adsorbed electron donor molecules (i.e., on the decrease in conductance caused by reducing chemicals) and vice versa (i.e., the increased conductance caused by electron acceptors on the surface, which induce p-type doping in WS_2). The results are consistent with sensing mechanisms recently proposed for TMDs [11, 13, 18]. The sensing performances of the present materials, however, are superior to those measured for WS_2 thin films [17] and comparable to the performance of MoS_2 and WS_2 flakes [10–14]. It is worth noting here that the parent WO_3 nanowires are n-type semiconductors that display an opposite sensing response to the same gas molecules [34].

The sensors show a very rapid response to all gases examined. The typical time constants are between 1 and 2 min at 200 ˚C, and slightly higher (~ 3–6 min) at lower temperatures. Since the gas response reflects the gas–solid interfacial equilibrium at the surface of WS_2, the faster response at higher temperatures can be expected, as a result of the increased reaction rates. A similar behavior was also found for the sensor recovery. The faster gas desorption and setting of the air–WS_2 equilibrium at the interface are the main drivers of the rapid sensor recovery at higher temperatures.

The sensor response to the analytes shows a nearly linear dependence on the gas concentration, with a slight decay in sensitivity at higher concentrations. The sensitivity to H_2S is particularly high (0.023 ppm^{-1}) compared to the other analytes (Fig. 3), which prompted us to carry out further tests on the WS_2–H_2S system.

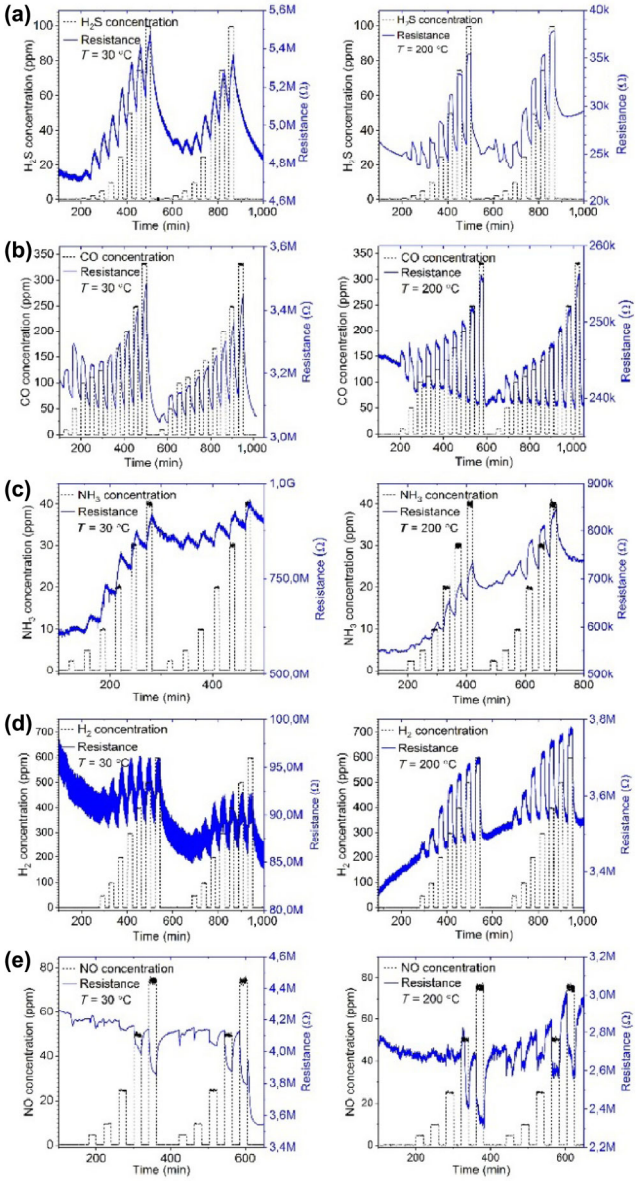

Figure 2 Sensor response to different analytes at part per million concentration levels. Responses measured both at 30 and 200 °C in (a) H_2S, (b) CO, (c) NH_3, (d) H_2, and (e) NO in air buffer. (Note: While the sensor devices used in our measurements are essentially the same, their overall resistance is different because of the inaccuracy of the amount of WS_2 nanomaterials deposited between the electrodes by drop casting.)

Exposing the sensor to sub-ppm H_2S levels revealed that the detection limit is as low as ~ 20 ppb at 200 ˚C, with a corresponding sensitivity of 0.043 ppm^{-1}.

To rationalize the present experimental findings and understand how H_2S interacts with WS_2, we carried out *ab initio* calculations using a simplified model involving single- and bilayer pristine/undoped WS_2. The calculations of the adsorption of H_2, CO, NO, and NH_3 were based on the work of Zhou et al. [18], who used first-principles simulations to determine the most favorable geometries of these molecules on monolayer WS_2. The same approach was followed in this work to estimate the adsorption energy of H_2S on WS_2 (see details in Table S2 in the ESM). The relaxed structure of H_2S adsorbed on the monolayer is shown in Fig. 4, whereas the results obtained for the other gas molecules are available in Figs. S2–S5 (in the ESM).

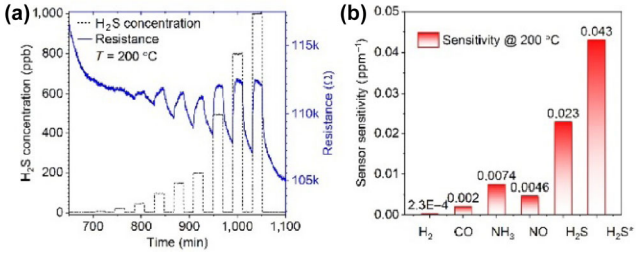

Figure 3 H_2S sensing performance at parts per billion levels. (a) Sensor resistance at 200 °C. (b) Sensitivity of the five different sensors, displaying high selectivity towards H_2S (0.023 ppm^{-1} at 1 ppm according to the data in Fig. 2). The data point labeled with an asterisk denotes the sensitivity (0.043 ppm^{-1}) measured at 20 ppb H_2S.

The adsorption energy of the gas molecules is calculated as: $E_{ads}[WS_2 + X] = E_T[WS_2 + X] - E_T[WS_2] - E_T[X]$, where $E_T[WS_2 + X]$, $E_T[WS_2]$, and $E_T[X]$ are the total energies of the supercell with the adsorbed molecule, the clean WS_2 slab, and the adsorbed molecule, respectively, in their optimized configuration. The calculated energies show that the adsorption of NO (–509.3 meV) is the most favorable among the systems investigated, followed by H_2S (–181 meV) and NH_3 (–171.7 meV). The adsorption energies of H_2 (–57.4 meV) and CO (–84.7 meV) are considerably smaller. The adsorption energies thus follow a similar qualitative trend as the experimental sensitivities, with the exception of NO (see Fig. 3(b)). This trend is

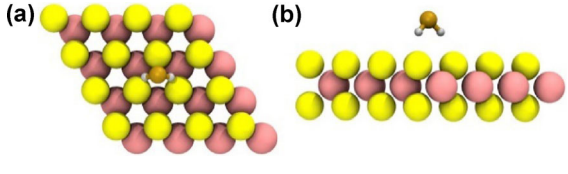

Figure 4 Relaxed structure of H_2S adsorbed on WS_2 monolayer. Top (a) and side (b) view of the most favorable DFT/PBE-D2 relaxed geometries for H_2S adsorbed on pristine WS_2 monolayer (Fig. S1 in the ESM). WS_2 and H_2S atoms are represented as yellow (S slab), ochre (S adsorbate), pink (W), and white (H) spheres.

also in agreement with previous calculations based on the local density approximation (LDA) [18]. The negative sign in the calculated adsorption energies indicates that all adsorption processes are thermodynamically favorable; moreover, higher absolute values denote higher binding with the slab. The present adsorption energies show some correlation with our experimental results on multilayered WS_2, which revealed good sensitivity towards H_2S (2.3×10^{-2} ppm^{-1}), ammonia (7.4×10^{-3} ppm^{-1}), and NO (4.6×10^{-3} ppm^{-1}), along with moderate sensitivity towards CO (2×10^{-3} ppm^{-1}) and H_2 (2.3×10^{-4} ppm^{-1}). Furthermore, the calculated E_{ads} of H_2S on the WS_2 bilayer shows a slight increase (–246.2 meV) with respect to that measured for the monolayer. This may suggest a qualitatively higher sensitivity towards H_2S in the case of the nanoflakes, compared with the monolayer. We also explored the possible intercalation of gas molecules between the adjacent WS_2 monolayers; however, our simple computational model predicts that the adsorption process is not energetically favorable in this case, due to the small interplanar distance between atoms in the adjacent layers (~ 3.1 Å) and the resulting repulsion between the S atoms belonging to the slab and the molecule. Nevertheless, we cannot rule out this possibility in the experiments, because structural defects in the material can provide perfect gates for the intercalation of gas molecules.

Electronic structure calculations were then carried out to understand the effects of the gas molecules on the electronic properties of WS_2. The band structure and density of states calculated for the H_2S molecule adsorbed on a WS_2 monolayer, shown in Fig. 5 (the results for the other gas molecules are available in Figs. S6–S9 in the ESM), are consistent with those reported in Ref. [18]. As shown in Fig. 5(a), the H_2S molecule has little influence on the band structure of WS_2 in the combined system, which remains almost the same as that of the pristine layer. The highest occupied molecular orbital (HOMO) of H_2S (green line in Fig. 5(a)) is located on the 2p orbital of the S atom and lies ~ 0.4 eV below the top of the valence band, as evidenced by a peak in the DOS curve (green line in Fig. 5(b)). The lowest unoccupied molecular orbital (LUMO) of H_2S lies approximately 2.9 eV above the top of the conduction band (not shown). Therefore, the H_2S molecule does not provide donor or acceptor states within the band gap of the WS_2 layer. The same behavior is observed in the case of H_2S adsorbed on bilayer WS_2 (Figs. 5(c) and 5(d)) and also for the other gases, with the exception of NO. In particular, our results show that only the NO molecule introduces three impurity levels within the band gap of WS_2, behaving as an acceptor (Fig. S8 in the ESM), in good agreement with the experiments.

Moreover, a Bader analysis was performed to study the local charge transfer associated with the adsorption of the gas molecules on the pristine WS_2 monolayer (Table S2 in the ESM). The results for H_2, CO, NH_3, and NO are in good agreement with previous data [18]. Accordingly, no sizable charge transfer is observed for H_2 and CO, and only a very small amount of charge is transferred in the case of NH_3 and NO. The NH_3 molecule acts as a donor by transferring 0.017 electrons to the monolayer, whereas the NO molecule acts as an acceptor, capturing 0.008 electrons. Similar to H_2 and CO, H_2S also exhibits very limited charge transfer over the pristine WS_2

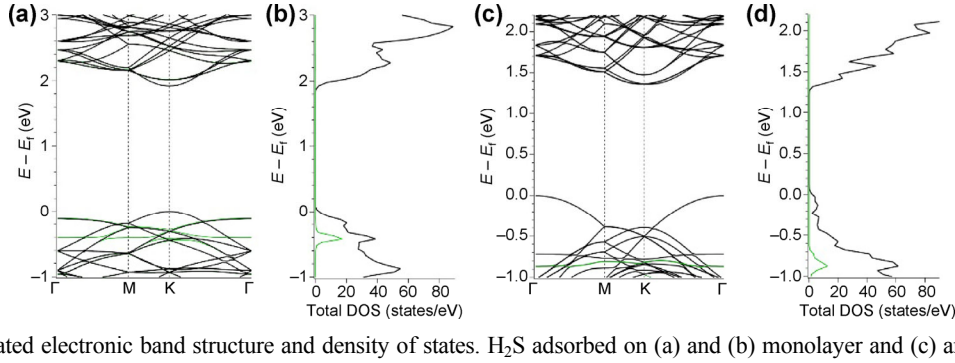

Figure 5 Calculated electronic band structure and density of states. H_2S adsorbed on (a) and (b) monolayer and (c) and (d) bilayer WS_2. The green lines represent the projections of the H_2S gas molecules.

slab, which indicates that the excellent sensitivity of the hybrid material towards the H_2S molecules observed in the experiments may have a different origin than the direct charge transfer within the clean monolayer. The minor amount of charge transfer observed for the most stable configuration is also compatible with the orbital mixing charge transfer theory. As discussed earlier, the mechanism of charge transfer between an adsorbate and a surface is partially governed by the mixing of the molecular HOMO and LUMO with the orbitals of the monolayer [35]. In the most favorable configuration of H_2S on pristine WS_2, the H atoms (LUMO) are oriented towards the monolayer, accepting electronic density from it. On the other hand, the HOMO of the molecule, located on the S atom, provides a slightly lower charge density to the slab because it is placed further away, resulting in a very small net charge transfer in the full system. We investigated the effect on the charge transfer of a H_2S molecule with the opposite orientation, i.e., with the H pointing away from the slab [35]. As expected, the direction of the charge transfer was inverted, and the gas molecule could be considered as a donor. This possibility cannot be ruled out for some of the adsorbates under the actual experimental conditions. However, in the case of the pristine WS_2 monolayer this configuration is clearly energetically unfavorable.

In order to identify any change in the surface chemistry of the materials during the gas sensing experiments that may affect their sensing response, we carried out X-ray photoelectron spectroscopy (XPS) measurements of the WS_2 hybrid nanostructures. Three samples were studied (Table 1): the original WS_2 hybrids (sample #1), the hybrid materials exposed to air at 200 °C for 1 h (sample #2), and those subsequently exposed also to H_2S at 200 °C for 1 h, in 1 ppm air (sample #3). The S $2p_{3/2}$ and O 1s peaks at around 162.3 and 530.7 eV (associated with WS_2 and WO_3, respectively) indicate the partial substitution of surface sulfur with oxygen when the WS_2 hybrid is heated in air. In addition, a new peak simultaneously appearing at 168.9 eV suggests the additional formation of sulfates, e.g., by the oxidation of sulfide and the reduction of O_2 to WO_3. On the other hand, when the sample is exposed again to H_2S (1 ppm in air), the sulfur concentration of the surface recovers the original value, despite the very low concentration of analyte.

According to a recent report, for 2D WS_2 nanoparticles the replacement of S with O occurs even at room temperature, resulting in the formation of some amorphous/crystalline WO_3 phase in the nanoflakes below/above 250 °C [36]. However, the very efficient and fast recovery of the WS_2 structure even after a short treatment in 1 ppm H_2S is unexpected and has important consequences for the sensing of H_2S in the presence of O_2 (e.g., in ambient air). As mentioned

Table 1 Surface composition of the WS_2 hybrid in various stages of the H_2S sensing process

Line	Sample #1 (Original WS_2 hybrid)			Sample #2 (WS_2 hybrid heated in air)			Sample #3 (sample heated in air and subsequently in 1 ppm H_2S)			Assignment
	BE (eV)	FWHM (eV)	AC (at.%)	BE (eV)	FWHM (eV)	AC (at.%)	BE (eV)	FWHM (eV)	AC (at.%)	
C 1s	284.2	1	8.53	284.3	1.05	9.99	284.3	0.85	3.52	W–C (?)
	285.3	1.25	3.34	285.3	1.1	3.38	285.3	1.45	3.93	C–(C, H)
O 1s	530.6	1.3	9.31	530.6	1.35	9.7	530.8	1.35	9.83	WO_3
	532.1	1.6	7.01	532.2	1.45	7.95	532.3	1.55	8.53	NaOH
	533.8	1.25	0.51	533.9	2	1.17	534.3	1.8	1.11	H_2O_{ads} (?)
Na 1s	1,071.7	1.7	6.28	1,071.7	1.65	7.78	1,071.9	1.6	7.44	NaOH
W $4f_{7/2}$	32.7	0.65	20.41	32.7	0.65	18.49	32.7	0.6	20.38	WS_2
	35.7	1.15	3.17	35.7	1.1	2.85	35.9	1.15	3.29	WO_3
S $2p_{3/2}$	162.3	0.65	41.44	162.3	0.65	37.28	162.4	0.6	41.94	WS_2
				168.9	1	1.42				SO_4^{2-}

above, the two extreme compositions, i.e., WO_3 and WS_2, have very different electrical characteristics: WO_3 is an n-type semiconductor, whereas WS_2 displays p-type semiconducting behavior. Accordingly, S doping in the WO_3 lattice or O doping in WS_2 are expected to cause significant changes in the electronic band structure and consequently alter the carrier localization upon adsorption of analyte gas molecules on the surface.

Therefore, the H_2S sensing process may be interpreted as a sequence of reversible adsorption/desorption and redox reactions, in which oxygen and sulfur compete for the anionic sites in the WS_2 lattice, thus modulating its band structure and electrical behavior, as schematically illustrated in Fig. 6.

In summary, our results indicate that the WS_2 nanohybrid possesses all key features (similar to other one-dimensional (1D) or 2D TMDs) to be applied as an effective gas sensor material, including a semiconducting nature and electrical transport properties adjustable via gas adsorption or (as observed in this study) lattice doping. Nevertheless, what renders the nanostructured hybrid probably superior to its 1D or 2D counterparts is the combination of the beneficial properties of nanowires and nanosheets. In particular, long 1D nanomaterials are preferred when electrically conductive networks need to be created between macroscopic electrodes. The long nanowires can establish percolation channels via a much lower number of interparticle connections than small zero-dimensional (0D) nanoparticles or 2D sheets [34, 37, 38]. This is particularly important, since during the electrical measurements the interfacial transport might dominate and suppress the effects of gas adsorption on the nanoparticles. On the other hand, small and thin 2D nanosheets have the fascinating ability to adsorb a significant fraction of surface-bound analytes not only on the 2D crystal facets but also on their edges [39], which may contribute to enhance the sensitivity of the 2D crystals, relative to other nanoparticles lacking edge adsorption sites.

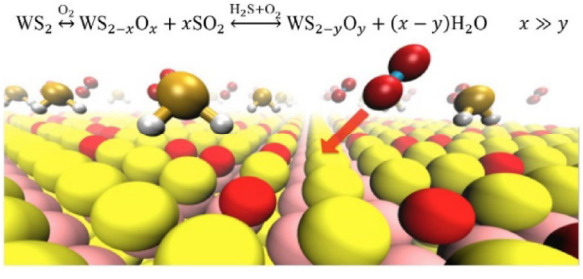

Figure 6 Schematic illustration of H_2S sensing mechanism on the surface of WS_2 in the presence of O_2. In the presence of air (O_2), the WS_2 lattice is doped with O, partially substituting S in the anionic sites. When even trace amounts of H_2S are added in the ambient gas, the O dopant is replaced with S until the equilibrium concentrations of O and S (which depend on the concentration of O_2 and H_2S in the surrounding gas) are reached.

4 Conclusions

The WS_2 nanowire-nanoflake hybrid materials investigated in this study were found to possess electrical properties highly sensitive to H_2S, along with moderate sensitivity to other analytes such as H_2, CO, NH_3, and NO in an air buffer. First-principles calculations based on the DFT-GGA approach with the PBE functional show that the intrinsic electronic properties of pristine WS_2 cannot fully explain its observed high sensitivity towards H_2S, whose origin might also be attributed to defects and/or doping in the WS_2 lattice. To test this possibility, we carried out XPS measurements on pristine and modified WS_2 nanowire-nanoflake hybrids and found that O_2 present in the environment during the sensor measurements induce a partial (and reversible) substitution of S by O at the anionic sites of the lattice, which may explain the high sensitivity and selectivity of the WS_2 nanowire-nanoflake heterostructures towards H_2S.

Acknowledgements

Funding received from Bio4Energy programme, Academy of Finland (projects Suplacat and ClintoxNP (No. 268944)), University of Oulu (More than Moore research community) and University of Oulu Graduate School (Infotech Oulu) is acknowledged. We acknowledge support from the EU (No. ERC-2016-AdG-694097 QSpec-NewMat) and the Basque Government "Grupos Consolidados UPV/EHU" (No. IT578-13). J. J. B. and L. D. X. thank the EU for the Marie Curie Fellowship (Nos. H2020-MSCA-IF-2016-751047 and H2020-MSCA-IF-2015-709382). A. P. P. thanks postdoctoral fellowship from the Spanish "Juan de la Cierva-incorporación" program (No. IJCI-2014-20147). We also would like

to acknowledge Sami Saukko (Center of Microscopy and Nanotechnology, University of Oulu) for his assistance with TEM analyses. A. L. S. acknowledges the Swedish Government Strategic Research Area in Materials Science on Functional Materials at Linköping University (Faculty Grant SFO-Mat-LiU No. 2009-00971).

Funding: Open access funding provided by Max Planck Society.

Electronic Supplementary Material: Supplementary material (reference data on resistive and FET H_2S gas sensors as well as details of calculated adsorption energies and equilibrium height values, relaxed geometries and corresponding electronic band structures upon gas adsorption for each analyte we studied in this work) is available in the online version of this article at https://doi.org/10.1007/s12274-018-2009-9.

References

[1] Neri, G. First fifty years of chemoresistive gas sensors. *Chemosensors* **2015**, *3*, 1–20.

[2] Devan, R. S.; Patil, R. A.; Lin, J. H.; Ma, Y. R. One-dimensional metal-oxide nanostructures: Recent developments in synthesis, characterization, and applications. *Adv. Funct. Mater.* **2012**, *22*, 3326–3370.

[3] Korotcenkov, G. Gas response control through structural and chemical modification of metal oxide films: State of the art and approaches. *Sens. Actuat. B Chem.* **2015**, *107*, 209–232.

[4] Palmisano, V.; Weidner, E.; Boon-Brett, L.; Bonato, C.; Harskamp, F.; Moretto, P.; Post, M. B.; Burgess, R.; Rivkin, C.; Buttner, W. J. Selectivity and resistance to poisons of commercial hydrogen sensors. *Int. J. Hydrogen Energy* **2015**, *40*, 11740–11747.

[5] Modi, A.; Koratkar, N.; Lass, E.; Wei, B. Q.; Ajayan, P. M. Miniaturized gas ionization sensors using carbon nanotubes. *Nature* **2003**, *424*, 171–174.

[6] Usha, S. P.; Mishra, S. K.; Gupta, B. D. Fiber optic hydrogen sulfide gas sensors utilizing ZnO thin film/ZnO nanoparticles: A comparison of surface plasmon resonance and lossy mode resonance. *Sens. Actuat. B Chem.* **2015**, *218*, 196–204.

[7] Chen, G. G.; Paronyan, T. M.; Pigos, E. M.; Harutyunyan, A. R. Enhanced gas sensing in pristine carbon nanotubes under continuous ultraviolet light illumination. *Sci. Rep.* **2012**, *2*, 343.

[8] Schedin, F.; Geim, A. K.; Morozov, S. V.; Hill, E. W.; Blake, P.; Katsnelson, M. I.; Novoselov, K. S. Detection of individual gas molecules adsorbed on graphene. *Nat. Mater.* **2007**, *6*, 652–655.

[9] Janata, J.; Josowicz, M. Conducting polymers in electronic chemical sensors. *Nat. Mater.* **2003**, *2*, 19–24.

[10] Kannan, P. K.; Late, D. J.; Morgan, H.; Rout, C. S. Recent developments in 2D layered inorganic nanomaterials for sensing. *Nanoscale* **2015**, *7*, 13293–13312.

[11] Li, B. L.; Wang, J. P.; Zou, H. L.; Garaj, S.; Lim, C. T.; Xie, J. P.; Li, N. B.; Leong, D. T. Low-dimensional transition metal dichalcogenide nanostructures based sensors. *Adv. Funct. Mater.* **2016**, *26*, 7034–7056.

[12] Perkins, F. K.; Friedman, A. L.; Cobas, E.; Campbell, P. M.; Jernigan, G. G.; Jonker, B. T. Chemical vapor sensing with monolayer MoS_2. *Nano Lett.* **2013**, *13*, 668–673.

[13] Cho, B.; Hahm, M. G.; Choi, M.; Yoon, J.; Kim, A. R.; Lee, Y.-J.; Park, S.-G.; Kwon, J.-D.; Kim, C. S.; Song, M. et al. Charge-transfer-based gas sensing using atomic-layer MoS_2. *Sci. Rep.* **2015**, *5*, 8052.

[14] Late, D. J.; Huang, Y.-K.; Liu, B.; Acharya, J.; Shirodkar, S. N.; Luo, J. J.; Yan, A. M.; Charles, D.; Waghmare, U. V.; Dravid, V. P. et al. Sensing behavior of atomically thin-layered MoS_2 transistors. *ACS Nano* **2013**, *7*, 4879–4891.

[15] Wang, Q. H.; Kalantar-Zadeh, K.; Kis, A.; Coleman, J. N.; Strano, M. S. Electronics and optoelectronics of two-dimensional transition metal dichalcogenides. *Nat. Nanotechnol.* **2012**, *7*, 699–712.

[16] Ko, K. Y.; Song, J.-G.; Kim, Y.; Choi, T.; Shin, S.; Lee, C. W.; Lee, K.; Koo, J.; Lee, H.; Kim, J. et al. Improvement of gas-sensing performance of large-area tungsten disulfide nanosheets by surface functionalization. *ACS Nano* **2016**, *10*, 9287–9296.

[17] O'Brien, M.; Lee, K.; Morrish, R.; Berner, N. C.; McEvoy, N.; Wolden, C. A.; Duesberg, G. S. Plasma assisted synthesis of WS_2 for gas sensing applications. *Chem. Phys. Lett.* **2014**, *615*, 6–10.

[18] Zhou, C. J.; Yang, W. H.; Zhu, H. L. Mechanism of charge transfer and its impacts on Fermi-level pinning for gas molecules adsorbed on monolayer WS_2. *J. Chem. Phys.* **2015**, *142*, 214704.

[19] Asres, G. A.; Dombovari, A.; Sipola, T.; Pskás, R.; Kukovecz, A.; Kónya, Z.; Popov, A.; Lin, J.-F.; Lorite, G. S.; Mohl, M. et al. A novel WS_2 nanowire-nanoflake hybrid material synthesized from WO_3 nanowires in sulfur vapor. *Sci. Rep.* **2016**, *6*, 25610.

[20] Ma, J. M.; Mei, L.; Chen, Y. J.; Li, Q. H.; Wang, T. H.; Xu, Z.; Duan, X. C.; Zheng, W. J. α-Fe_2O_3 nanochains: Ammonium acetate-based ionothermal synthesis and ultrasensitive sensors for low-ppm-level H_2S gas. *Nanoscale* **2013**, *5*, 895–898.

[21] Li, Z. J.; Huang, Y. W.; Zhang, S. C.; Chen, W. M.; Kuang, Z.; Ao, D. Y.; Liu, W.; Fu, Y. Q. A fast response & recovery H_2S gas sensor based on α-Fe_2O_3 nanoparticles with ppb level detection limit. *J. Hazard. Mater.* **2015**, *300*, 167–174.

[22] Manorama, S.; Devi, G. S.; Rao, V. J. Hydrogen sulfide sensor based on tin oxide deposited by spray pyrolysis and microwave plasma chemical vapor deposition. *Appl. Phys. Lett.* **1994**, *64*, 3163–3165.

[23] Kneer, J.; Knobelspies, S.; Bierer, B.; Wöllenstein, J.; Palzer, S. New method to selectively determine hydrogen sulfide concentrations using CuO layers. *Sens. Actuat. B Chem* **2016**, *222*, 625–631.

[24] Zhang, F.; Zhu, A. W.; Luo, Y. P.; Tian, Y.; Yang, J. H.; Qin, Y. CuO nanosheets for sensitive and selective determination of H_2S with high recovery ability. *J. Phys. Chem. C* **2010**, *114*, 19214–19219.

[25] Li, Y. H.; Luo, W.; Qin, N.; Dong, J. P.; Wei, J.; Li, W.; Feng, S. S.; Chen, J. C.; Xu, J. Q.; Elzatahry, A. A. et al. Highly ordered mesoporous tungsten oxides with a large pore size and crystalline framework for H_2S sensing. *Angew. Chem., Int. Ed.* **2014**, *53*, 9035–9040.

[26] Li, Z. J.; Niu, X. Y.; Lin, Z. J.; Wang, N. N.; Shen, H. H.; Liu, W.; Sun, K.; Fu, Y. Q.; Wang, Z. G. Hydrothermally synthesized CeO_2 nanowires for H_2S sensing at room temperature. *J. Alloy. Comp.* **2016**, *682*, 647–653.

[27] Li, M.; Zhou, D. X.; Zhao, J.; Zheng, Z. P.; He, J. G.; Hu, L.; Xia, Z.; Tang, J.; Liu, H. Resistive gas sensors based on colloidal quantum dot (CQD) solids for hydrogen sulfide detection. *Sens. Actuat. B Chem.* **2015**, *217*, 198–201.

[28] Perdew, J. P.; Burke, K.; Ernzerhof, M. Generalized gradient approximation made simple. *Phys. Rev. Lett.* **1996**, *77*, 3865–3868.

[29] Giannozzi, P.; Baroni, S.; Bonini, N.; Calandra, M.; Car.; R.; Cavazzoni, C.; Ceresoli, D.; Chiarotti, G. L.; Cococcioni, M.; Dabo, I. et al. QUANTUM ESPRESSO: A modular and open-source software project for quantum simulations of materials. *J. Phys. Condens. Matter* **2009**, *21*, 395502.

[30] Grimme, S. Semiempirical GGA-type density functional constructed with a long-range dispersion correction. *J. Comput. Chem.* **2006**, *27*, 1787–1799.

[31] Hartwigsen, C.; Goedecker, S.; Hutter, J. Relativistic separable dual-space Gaussian pseudopotentials from H to Rn. *Phys. Rev. B* **1998**, *58*, 3641–3662.

[32] Monkhorst, H. J.; Pack, J. D. Special points for Brillouin-zone integrations. *Phys. Rev. B* **1976**, *13*, 5188–5192.

[33] Tang, W.; Sanville, E.; Henkelman, G. A grid-based Bader analysis algorithm without lattice bias. *J. Phys. Condens. Matter* **2009**, *21*, 084204.

[34] Kukkola, J.; Mohl, M.; Leino, A.-R.; Mäklin, J.; Halonen, N.; Shchukarev, A; Konya, Z.; Jantunen, H.; Kordas, K. Room temperature hydrogen sensors based on metal decorated WO_3 nanowires. *Sens. Actuat. B Chem.* **2013**, *186*, 90–95.

[35] Leenaerts, O.; Partoens, B.; Peeters, F. M. Adsorption of H_2O, NH_3, CO, NO_2, and NO on graphene: A first-principles study. *Phys. Rev. B* **2008**, *77*, 125416.

[36] Perrozzi, F.; Emamjomeh, S. M.; Paolucci, V.; Taglieri, G.; Ottaviano, L.; Cantalini, C. Thermal stability of WS_2 flakes and gas sensing properties of WS_2/WO_3 composite to H_2, NH_3 and NO_2. *Sens. Actuat. B Chem.* **2017**, *243*, 812–822.

[37] Kukkola, J.; Mohl, M.; Leino, A.-R.; Tóth, G.; Wu, M.-C.; Shchukarev, A.; Popov, A.; Mikkola, J.-P.; Lauri, J.; Riihimäki, M. et al. Inkjet-printed gas sensors: Metal decorated WO_3 nanoparticles and their gas sensing properties. *J. Mater. Chem.* **2012**, *22*, 17878–17886.

[38] Kukkola, J.; Mäklin, J.; Halonen, N.; Kyllönen, T.; Tóth, G.; Szabó, M.; Shchukarev, A.; Mikkola, J.-P.; Jantunen, H.; Kordás, K. Gas sensors based on anodic tungsten oxide. *Sens. Actuat. B Chem.* **2011**, *153*, 293–300.

[39] Cha, J.-H.; Choi, S.-J.; Yu, S.; Kim, I.-D. 2D WS_2-edge functionalized multi-channel carbon nanofibers: Effect of WS_2 edge-abundant structure on room temperature NO_2 sensing. *J. Mater. Chem. A* **2017**, *5*, 8725–8732.